Loughborough University

This item was submitted to Loughborough's Research Repository by the author.
Items in Figshare are protected by copyright, with all rights reserved, unless otherwise indicated.

Critical trajectories for aerosol particles: their determination for impaction in fibrous filters and in oscillating bubbles

PLEASE CITE THE PUBLISHED VERSION

http://dx.doi.org/10.1016/j.jaerosci.2013.12.004

PUBLISHER

© Elsevier

VERSION

AM (Accepted Manuscript)

LICENCE

CC BY-NC-ND 4.0

REPOSITORY RECORD

Clement, Charles F., and Sarah J. Dunnett. 2014. “Critical Trajectories for Aerosol Particles: Their Determination for Impaction in Fibrous Filters and in Oscillating Bubbles”. figshare. https://hdl.handle.net/2134/14182.

Loughborough University

This item was submitted to Loughborough's Institutional Repository (https://dspace.lboro.ac.uk/) by the author and is made available under the following Creative Commons Licence conditions.

creative commons

COMMONS DEED

Attribution-NonCommercial-NoDerivs 2.5

You are free:

- to copy, distribute, display, and perform the work

Under the following conditions:

Attribution. You must attribute the work in the manner specified by the author or licensor.

Noncommercial. You may not use this work for commercial purposes.

No Derivative Works. You may not alter, transform, or build upon this work.

- For any reuse or distribution, you must make clear to others the license terms of this work.
- Any of these conditions can be waived if you get permission from the copyright holder.

Your fair use and other rights are in no way affected by the above.

This is a human-readable summary of the Legal Code (the full license).

Disclaimer

For the full text of this licence, please go to:
http://creativecommons.org/licenses/by-nc-nd/2.5/

Critical Trajectories for Aerosol Particles: Their Determination for Impaction in Fibrous Filters and in Oscillating Bubbles

C. F. Clement[1] and S. J. Dunnett[2]

[1]15 Witan Way, Wantage, Oxon, OX12 9EU, U.K.

[2]Department of Aeronautical and Automotive Engineering, Loughborough University, Loughborough, Leics.

LE11 3TU, U.K.

Keywords: fibrous filter, filtration, numerical simulation, particle deposition

Abstract

Critical trajectories for aerosol particles in a gas flow are ones which divide an aerosol flux into different parts, for example aerosol which is, and is not deposited. They can exist in all gas flows in which aerosol motion is governed by gas velocity rather than by diffusion and we describe two mathematical methods for their calculation. For deposition by impaction on a filter fibre it is necessary to solve the differential equations for particle motion and an efficient iterative procedure is used to obtain the critical trajectories.

Jonas and Schütz (1988) have shown that aerosol impaction is an important mechanism for the removal of aerosol from an oscillating sodium vapour bubble formed during a hypothetical core disruptive accident in a fast reactor. For these one-dimensional oscillations, when the gas velocity within a bubble is a linear function of position, we extend their work by calculating critical trajectories directly from the integral equation describing a depositing particle for two models with different initial conditions. With initially entrained uniform aerosol, the percentage impacted is independent of the inclusion of gravity in the calculations as long as regions empty of aerosol do not appear in the bubbles. Numerical results are obtained for a wide range of amplitudes of bubble oscillations and aerosol in the size range 1-30 μm. In agreement with Jonas and Schütz, we find that a considerable fraction of the aerosol at larger sizes is removed by impaction. For aerosol below 20 μm in size, the removal fraction does not always increase with the oscillation amplitude, but appears to peak at a certain value of the amplitude. This could indicate a kind of resonant behaviour coupling aerosol entrainment to oscillations in the gas velocity. The theory is applicable to different types of bubble oscillation.

1. Introduction

Critical trajectories for aerosol particles which divide different outcomes for the particles can exist in all gas flows in which aerosol motion is governed by gas velocity rather than by diffusion, namely for all except small particles at low velocities. They are important in many flows leading to aerosol deposition, aerosol impaction, and aerosol selection, and, for filtration, their importance was recognised by Davies (1973). Their calculation enables the parameters of the flow and particle characteristics for particular outcomes to be found without calculating large numbers of aerosol trajectories, and would have applications to large scale calculations of aerosol motion involving rebound (Tu *et al* 2004) and for aerosol entering and passing into the human respiratory system (Lai *et al* 2008, 2013). The determination of particle trajectories by solution of their equation of motion in a given flow field was discussed by Davies (1973), and here we describe a very efficient method for reaching the limiting critical trajectory for impaction in a fibrous filter by a process of iteration. We also describe a direct method for their determination applicable to impaction in an oscillating gas bubble inside a liquid in which the equations in a time-dependent velocity field can be transformed into an integral equation.

In both cases the flow field in which the particles move must be known or calculable, and we assume the particles are subject to Stokes' drag in conditions such that the Stokes number, $St \geq 1$ so that diffusion can be neglected in describing the particle motion.

In our previous work on filtration (Dunnett and Clement 2006, 2009 and 2012), the boundary element method was used to calculate the flow field for aerosol particles incident on a fibre. The deposition mechanisms examined for a growing deposit were diffusion (Dunnett and Clement 2006) and also interception (Dunnett and Clement 2009, 2012). The aim of calculating limiting critical trajectories in the same flow field is to extend this work to deposition by impaction where these trajectories are ones for which particles just touch the growing deposit surface. Once these limiting trajectories are known, it is possible to determine the deposition pattern within a filter and the filter efficiency as deposit is collected. The iterative method described in section 2 to determine these trajectories is based on Newton's method used to determine zeros of a function. We find that it is very efficient and only a few iterations are necessary to determine a critical trajectory.

A large bubble consisting mainly of sodium vapour could be formed during a hypothetical core disruptive accident (HCDA) in a liquid-metal-cooled fast breeder reactor (LMFBR). This bubble would initially be under the surface of the sodium, but could transport radioactive aerosol from the core to give a 'primary or HMA bubble source term' in the inner reactor containment. The possible magnitude of this source term has been the subject of simulant experiments (Berthoud et al 1988), and impaction and washout mechanisms have been identified as contributing substantial amounts to removal of aerosol from the bubble (Jonas and Schütz 1988). In this paper, we contribute to the theory needed to quantify the removal rates, in

particular by showing how aerosol removal by impaction may be efficiently calculated for certain realistic types of bubble oscillation.

Aerosol trajectories in a time-dependent gas velocity field can be calculated from the equation of motion of a particle in the field. In section 3, we describe how critical trajectories which impact into walls at specified times can be calculated for fields which are linear in position, but arbitrary functions of time. Such fields naturally describe gas flows required to keep the pressure uniform for a wide class of rapid bubble oscillations. These include the one-dimensional motion considered by Jonas and Schütz (1988) which is described here.

The equation of motion for a spherical aerosol particle is taken from Jonas and Schütz (1988), and the thermodynamic functions needed to perform calculations in high temperature sodium vapour are summarised in Appendix A. Calculations are restricted to the Stokes drag regime for aerosol up to 30μm in radius.

Equations with, and without, gravity included are considered to see when results for impaction should correspond. Remarkably, the impaction percentage from an initially uniform entrained aerosol is unchanged if none of the gas space becomes empty of aerosol.

The basic theory is described in section 3 and involves formally integrating the equation of motion so that initial and final boundary conditions are incorporated into the resulting integral equation. For linear velocity fields, the integral equation is linear, so that final positions along trajectories can be scaled from initial positions. This process makes it easy to identify critical trajectories and directly calculate percentages of aerosol impacted, and the proportions of the cavity which are empty and filled with aerosol of a given size at any time.

In section 4, we show that a similar theory applies to the calculation of deposition in radial oscillations of a spherical bubble to calculate percentages of aerosol deposited by impaction. Some extensions of the theory to more complex bubble oscillations are also considered.

The calculations described in section 5 were originally made in unpublished work by Robin Clement in the 1990s. Two models were introduced to represent limiting cases for aerosol inside an oscillating bubble. In the first model (I) the aerosol is initially entrained at the maximum gas velocity and in the second model (II) entrained at the minimum (zero) velocity. As initial conditions in bubbles formed in possible accidents might not be well specified, these models would bracket all possibilities. This uncertainty was not considered by Jonas and Schütz (1988).

It is not easy to integrate numerically the integral equation for the whole range of parameters considered because rapidly varying exponential functions are involved. A numerical scheme that has proved to be satisfactory is described in Appendix B. Results for calculations using both models are given in section 5. For model 1, where no empty regions appear in the bubble, results for the percentage of aerosol impacted

are given as functions of aerosol size, oscillation amplitude, and time during an oscillation. In model II, where empty regions do appear, results for their percentage size are also given.

Finally, in the conclusions in section 5, we summarize the results obtained and point out some other possible applications of the theory including deposition in aerosol passage to the lung.

2. Critical trajectories for impaction on a fibre.

In the case of aerosol filtration with particles such that the Stokes number, St > 1, inertial impaction will be the main mechanism of capture. The Stokes number is given by $St = d_p^2 \rho_p U_0 C / (8 \mu d_f)$; d_p, d_f are the particle and fibre diameters, ρ_p the particle density, C the Cunningham correction factor, and μ the air viscosity.

The critical trajectories separate those particles that will impact the filter from those that do not, and are tangential to the fibre surface at impact, see Figure 1. Away from the fibre particles are initially moving with the flow in the x direction with velocity $u = U_0$ and the problem of finding the critical trajectory reduces to that of finding the distance from the axis, y_0, for a trajectory to reach the appropriate tangential boundary condition on the fibre surface. This reduces to solving the differential equations for a trajectory which satisfy a particular boundary condition. The equations for a trajectory in a two-dimensional flow field (U(x,y), V(x,y)) shown in Fig.1 are

$$d^2x / dt^2 + \beta\, dx / dt = \beta\, U(x,y)$$
$$d^2y / dt^2 + \beta\, dy / dt = \beta V(x,y), \qquad (1)$$

where $\beta = 1 / 2St$.

These equations are immediately integrable to determine the particle velocity, u = dx / dt and v = dy / dt., and these first order equations are then integrated to determine the trajectory. At the point (x_m, y_m), where the critical trajectory meets the fibre, its direction, given by ($u(x_m, y_m)$, $v(x_m, y_m)$) is tangential to the fibre surface $R_f(x_m, y_m)$. To use Newton's iterative method to determine y_0 from this point, we need to define a function, $R_{min}(y_0)$ which is zero at the point and changes from positive to negative for trajectories which miss and impact the fibre, respectively. For non-intersecting trajectories we take this to be the minimum distance of the trajectory from the fibre surface,

$$R_{min} = (x^2 + y^2)^{1/2} - R(\theta), \qquad (2)$$

where $\tan\theta = y/x$ and (x, y) is the point on the trajectory closest to the fibre..

For intersecting trajectories, we define R_{min} to be the negative value of the distance from the fibre surface to the chord crossing the fibre from the point of intersection along the fibre radius perpendicular to the chord, as shown in Fig.2. The direction of the chord is parallel to the particle velocity vector at the point of intersection. The value of R_{min} is a function of y_0 and, the Newton's iterative procedure to find successive values is given by

$$y_0(2) = y_0(1) + R_{min}(y_0(1)) / (dR_{min}(y_0(1)) / dy_0), \quad (3)$$

where $y_0(2)$ is an improved value from $y_0(1)$.

The procedure has been tested using trajectory calculations with flow fields calculated by the boundary element method (Dunnett and Clement 2006). In Figures 3 and 4 we show results for two cases of impaction on clean fibres:

A. d_f = 40 μm, d_p = 3.6 μm, U_0 = 1 ms^{-1} with St = 1.0889,

B. d_f = 40 μm, d_p = 3.6 μm, U_0 = 4.59 ms^{-1} with St = 5.

The results for case A are labelled y1 in Figure 3 and for case B as y2. Figure 3 shows the values of y_0 plotted against iteration number N. The lengths used in the calculations are in units of fibre radius so that the starting choice of y_0 = 1 for the iterations is unrealistically far from the value for the critical trajectory for case A. Nevertheless, convergence to an accurate final value is very rapid for both cases as shown in Figure 3. Figure 4 shows the corresponding values of R_{min} for case A where the limiting value is approached from impacting trajectories with negative values of R_{min}. Values of R_{min} are not shown for case B as they are very small after the first iteration. The critical values of y_0 reached in Fig. 3 also shows that far more aerosol (amount proportional to y_0^2) impacts at the higher velocity of Case B. We will investigate the case of impaction and its effect on the efficiency of aerosol filtration more fully in the future, but it is clear that the iterative procedure adopted works very well in determining limiting trajectories.

3. Critical trajectories for bubble oscillation in one dimension

Aerosol particles or droplets impact into walls when they cannot follow accelerations in gas flow. The relevance to bubbles under sodium is that their walls will initially be in rapid motion because of the large pressure difference with the cover gas space. This subject is well described by Jonas and Schiltz (1988) so that the description here is confined to the use of critical trajectories which can improve upon their method of calculation.

If, at any time, we can determine the trajectory of an aerosol particle from an initial configuration that is just impacting a wall, we will be able to tell from the initial geometry a set of trajectories for particles of the same size that have already impacted into the wall. We show here that such critical trajectories can be calculated by constructing an integral equation for the aerosol motion when the gas velocity is linear in spatial co-ordinates whilst still being an arbitrary function of time. This covers motion at uniform pressure in one dimension, the case considered by Jonas and Schütz (1988).

The motion of a spherical aerosol particle of radius R moving in a gas in motion with a velocity **u**(**r**,t) is (Jonas and Schütz 1988),

$$d\mathbf{v} / dt = (\pi / 2m_d) \rho_v C_D R^2 \, | \mathbf{u} - \mathbf{v} | (\mathbf{u} - \mathbf{v}) - \mathbf{g} \quad (4)$$

where g is the gravitational acceleration, ρ_v is the gas (sodium vapour) density, and the aerosol mass is

$$m_d = 4 \pi \rho_p R^3 \quad (5)$$

The drag coefficient, C_D, is given in terms of the Reynolds number,

$$Re=2 \mid \mathbf{u} - \mathbf{v} \mid R / \nu_v, \quad (6)$$

by

$$C_D = 24/Re, \qquad 10^{-5} \le Re \le 0.25 \quad (7)$$

$$= 21/Re + 6 / Re^{1/2} + 0.28, \qquad 0.25{:}5 \le Re \le 4000 \quad (8)$$

$$= 24/Re + 0.5 \qquad 4000 < Re \quad (9)$$

In (6), ν_v, = η_v / ρ_v is the kinematic viscosity of the gas, whose magnitude for sodium vapour is described in Appendix A. In this section we are interested in aerosol in the size range between about 1 and 30 μm, which is mainly governed by the Stokes drag (7). Corrections to (4) at the smallest sized end from the Cunningham slip correction included by Jonas and Schütz (1988) are ignored here.

For vertical motion in one dimension, the case we consider first, eq (4) in the Stokes regime (7) reduces to

$$d^2z / dt^2 + \alpha \, dz / dt = \alpha \, u(z,t) - g \quad (10)$$

where the particle response to changes in gas velocity u is given by the parameter,

$$\alpha = 9 \, \eta_v / (2 \, \rho_p \, R^2) \quad (11)$$

At a temperature of 1000 ^{0}C, $\eta_v = 1.34 \, 10^{-5}$ kg m^{-1} s^{-1}, which gives, with $\rho_p = 4.5 \, 10^3$ kg m^{-3} corresponding to a CsI particle,

$$\alpha = 1.34 \, 10^4 / R^2 (\mu m) \, s^{-1} \quad (12)$$

which is the value that we adopt here for calculations. Its value would decrease with an increase of temperature, as the viscosity increases, and would also be smaller for denser particles, e.g. over a factor of 2 smaller for actinide particles.

For a cavity of height, Z(t), whose base is fixed, the gas velocity required to keep the pressure uniform is

$$u = (z / Z(t)) \, dZ / dt \quad (13)$$

This is the form used by Jonas and Schütz (1988). The behaviour of Z(t) which increases from Z_0 by an amount Z_1 and then decreases is shown in Figure 5. A critical trajectory of an aerosol particle starting from an initial value, z = Z_0 is shown in Fig. 5a. This divides the space into a region where all aerosol impacts the wall up to time t, and a region where no aerosol meets the wall. Clearly, if the critical trajectory can be calculated, the proportion of an initial aerosol removed by impaction is immediately determined.

Initially, the top of the cavity may move away from the aerosol, and an empty region appears as shown in Fig. 5(b). There can then be impaction for a certain time, but an empty region may reappear. The proportion of aerosol impacted and the boundaries of the regions can be found if the limiting trajectories, $Z_i(t)$ and $Z_m(t)$, can be calculated.

We first prove that, under certain conditions, this removal proportion is independent of gravity. Referring to Figure 6, we describe the critical trajectories which impact the top and bottom boundaries, and subtract their equations corresponding to (7). With or without gravity, we obtain the identical equation (the factor g cancels),

$$d^2 \Delta z / dt^2 + \alpha \, d\Delta z / dt = \alpha \, (\Delta z / Z(t)) \;\; dZ / dt \qquad (14)$$

Solutions of this equation are the same in the two cases corresponding to critical trajectories (Δz_i same, $\Delta z_f = Z_f$ same) provided that the initial velocities are identical. If the aerosol is initially moving with the gas, we have for the two cases:

$$\text{(a)} \qquad d\Delta z / dt \,\big|_{t=0} = (z_c / z_0) \, dZ(0)/dt = (\Delta z_i / Z_0) \, dZ(0)/dt$$

$$\text{(b)} \qquad d\Delta z / dt \,\big|_{t=0} = (z_{ct} - z_{cb}) / z_0) \, dZ(0)/dt = (\Delta z_i / Z_0) \, dZ(0)/dt \qquad (15)$$

Thus, with this condition on the initial aerosol velocity, the addition of gravity does not change the removal proportion and, for simplicity, we shall omit g from eq. (10) in subsequent calculations here. In general, the result holds only so long as no part of the gas space becomes completely empty of aerosol, i.e. a critical trajectory exists at both boundaries. For example, for gravity alone and a fixed cavity, the top boundary of the aerosol moves down with time away from the roof. Referring to Fig. 6, the result would hold only if the top trajectory with gravity included meets Z(t) between t_i and t_m, and then only between this meeting time and the time an empty region next appears.

We now obtain a formal solution to eq. (10). Integrating once,

$$dz / dt + \alpha \, z = dz(o) / dt + \alpha z + \alpha \int_0^t dt \, [z(t') / Z(t')] \, dZ(t') / dt \qquad (16)$$

Again, this can be formally integrated using the integrating factor $e^{\alpha t}$ to obtain,

$$z \exp(\alpha t) - z_0 = (dz(0) / dt + \alpha \, z_0) \, (\exp(at) - 1) / \alpha$$

$$+\alpha \int_0^t dt' \exp(\alpha t') \int_0^{t'} dt'' \, [z(t'') / Z(t'')] \, dZ(t'') / dt \qquad (17)$$

The final integral is reduced to a single integral by interchanging the order of integration:

$$z = z_0 + dz(o) / dt \, [1 - \exp(-\alpha t)] / \alpha + \int_0^t dt' \, [1 - \exp[-\alpha(t - t')]] \, [z(t') / Z(t')] \, dZ(t')/dt \qquad (18)$$

It is convenient to divide z into the part committed by the initial velocity and the residual, so that

$$z / z_0 = 1 + (1 / z_0) \, dz(o)/dt \, [1 - \exp(-\alpha t)] / \alpha + x \qquad (19)$$

Equations for $X = x/z_0$ are then, from (18),

$$X = \int_0^t dt' \, [1 - \exp(-\alpha(t - t'))] \, [B(t') + X(t') l \, f(t') \qquad (20)$$

or, differentiating,

$$dX / dt = \alpha \, t \int_0^t dt' \exp(-\alpha(t - 0) \, [B(t') + X(t') l \, f(t') \qquad (21)$$

where, for an initial velocity of u given by eq. (13),

$$B(t) = 1 + (1 / Z_0) \, dZ(o) / dt \;\; (1 - \exp(-\alpha t)) / \alpha \qquad (22)$$

$$f(t) = (1 / Z(t)) \, dZ / dt \qquad (23)$$

These functions determine the critical trajectory for which z = Z(t) at time t and the corresponding fraction of aerosol not impacted:

$$z_0 / Z_0 = (z_0 / Z(t)) (Z(t) / Z_0) = (Z(t) / Z_0) / (B(t) + X(t)) \quad (24)$$

The fraction of aerosol impacted at time t is thus

$$P_1 = [1 - (Z(t) / Z_0) / (B(t) + X(t))] \times 100\% \quad (25)$$

If an empty region appears initially (Fig. 5 b), its size can be obtained from the top trajectory which starts at $z_0 = Z_0$ i.e.

$$z / Z(t) = (z / Z_0) (Z_0 / Z(t)) = (B(t) + X(t)) Z_0 / Z(t) = P_0 / 100 \quad (26)$$

where P_0 is the percentage height occupied by aerosol.

The percentage empty is given by

$$P_E = 100 - P_0. \quad (27)$$

For a second empty region following impaction as in Fig. 5b, we first calculate the maximum fraction impacted from eq. (24) with $t = t_m$ and $z_0 = z_{0m}$. The fraction full of aerosol at a later time now corresponds to $z_0 = z_{0m}$ so that

$$z / Z(t) = (z / z_{0m}) (z_{0m} / Z(t)) = (B(t) + X(t))(Z_0 / Z(t)) z_{0m} / Z_0 = P_0 / 100. \quad (28)$$

This result is just obtained from (23) by multiplying by the fraction, z_{0m}/ Z_0, of initial aerosol not impacted or by $1 - P_I/100$.

4. Oscillating spherical bubbles

We consider aerosol inside a spherical bubble of radius $R_s(t)$ which expands and contracts. Within the bubble, the radial gas velocity required to keep the pressure and density uniform is

$$u_r = (r / R_s) dR_s / dt \quad (29)$$

where the gas density and pressure (at constant temperature) are proportional to R_s^{-3}.

The general equation for aerosol trajectories subject to Stokes drag is now

$$d^2\mathbf{r} / dt^2 + \alpha\, d\mathbf{r} / dt = \alpha\, \mathbf{u} - \mathbf{g} \quad (30)$$

where, from (26), the velocity **u** has the Cartesian components.

$$(u_x, u_y, u_z) = (1 / R_s) dR_s(x, y, z) /dt \quad (31)$$

It can again be proved that, subject to the existence of critical trajectories and no part of the volume being completely denuded of aerosol, the fractional volume of the initial bubble cleared of aerosol by impaction is independent of whether or not gravity is included in the calculation. We can proceed to calculate impaction in the bubble without gravity when eq.(29) in the radial coordinate becomes

$$d^2 r / dr^2 + \alpha\, dr / dt = \alpha\, (r / R_s) dR_s /dt, \quad (32)$$

$$X(t) = r / r_0 - 1 - (1 / r_0)\ dr(o)/dt[1 - \exp(-at)] / \alpha\ , \quad (33)$$

$$f(t) = (1 / R_s(t)) dR_s(t) /dt \quad (34)$$

Because the sphere is in three dimensions, the fraction of aerosol impacted at time t is obtained by replacing eqs. (24) and (25) by

$$r_o / R_s (0) = (R_s (t) / R_s(0)) / (B(t) + X(t)), \quad (35)$$

$$P_I = \{ 1 – [(R_s (t) / R_s(0)) / (B(t) + X(t))]^3\} \text{ x } 100\%, \quad (36)$$

Similar generalizations can be made to eqs. (26) and (28).

The technique used for solving the general equation (32) can be generalized to other bubble geometries provided that independent linear equations for the trajectories in x, y and z are obtained with the appropriate gas flow **u**. This implies that the most general form for **u** is

$$(u_x, u_y, u_z) = (f_x(t)x, f_y(t)y, f_z(t)z) \quad (37)$$

where the $f_i(t)$ are solely functions of time but may differ for the different components.

The minimum general requirement on the flow velocity is that it must satisfy the continuity equation

$$- (1 / \rho) d\rho / dt = \nabla.\mathbf{u} = f_x(t) + f_y(t) + f_z(t), \quad (38)$$

where ρ is the gas density in the bubble.

Thus, for a velocity of the form (37), ρ is constrained to be uniform within the bubble. This is the natural response to pressure changes arising from any motion of bubble walls at much less that the speed of sound in the gas and so will always be approximately satisfied in practice. We note that allowing $f_x(t)$ to be a function of y and z would violate this requirement.

The crucial additional requirement for the theory is that, at limiting values of x, y and z, **u** given by (37) must describe the motion of boundary walls. This immediately implies that, for solid walls where the component of **u** perpendicular to the wall must vanish, there are only the following cases:

(i) If there is some motion perpendicular to the wall, the wall must be a plane, e.g. x = 0, and there is no other parallel wall.

(ii) For two plane parallel walls, there is no motion between them e.g. x = 0 and x = L when $f_x(t) = 0$.

(iii) For two non-parallel plane walls, or for a non-planar two-dimensional wall, motion is only possible in the one dimension along the walls, e.g. the z direction for walls x = 0, x = y, or for the wall x = g(y), where g is a non-linear function of y.

The cases (i) include the interesting possibilities of motion out of a right-angled edge or corner.

For unconstrained bubble motion, we would normally expect the motion and boundaries to be symmetric about the origin. A most important possibility and generalization of the above work is that eq. (38) allows for bubble oscillations at constant pressure, volume and density when

$$f_x(t) + f_y(t) + f_z(t) = 0 \quad (39)$$

As an example, we consider the motion of a 2D ellipse, which is easily generalized to a 3D ellipsoid, whose surface is given by

$$x^2/ a^2 + y^2/ b^2 =1. \quad (40)$$

A general point on the surface is given by

$$x = a \cos s, \qquad y = b \sin s. \tag{41}$$

For oscillatory motion of the surface, we allow a and b to become functions of time, when we find

$$(u_x,\ u_y) = [(1 / a)\ da/dt, (1 / b)\ db/dt, \tag{42}$$

corresponding to surface motion

$$dx / dt = \cos s\ da/dt, \qquad dy / dt = \sin s\ db/dt \tag{43}$$

The condition (39) does not have to be satisfied for solutions to be obtained, but, with $f_x(t) = (l/a)(da/dt)$, corresponds to the constant area condition ab = constant. The method introduced above to calculate aerosol impaction in an oscillating 1D bubble, can be used to calculate impaction in volume-conserving oscillations of 2 or 3D bubbles induced, for example, by pressure waves passing through a liquid.

5. Calculations

For bubbles under liquid sodium, their motion will be determined by pressure variation which is governed by the inertia of -the sodium and the pressure response of the cover gas (Jonas and Schütz 1988). Consequent multiple oscillations could be strongly damped by condensation (see, for example, Knowles and Turrel 1991), so that calculations here are restricted to simple models with just one major oscillation. We describe the calculational method first and give some results obtained. We have performed calculations with two models for Z(t), representing different initial conditions in both of which, however, the aerosol is assumed to have the initial motion of the gas:

Model 1

$$Z(t) = Z_0(1 + h \sin\omega t), \quad 0 \le t \le \pi / \omega. \tag{44}$$

Model II

$$Z(t) = Z_0\ (1 - h \cos\omega t)/ (1 – h), \quad 0 \le t \le 2\pi / \omega. \tag{45}$$

In both cases the initial cavity size is Zo, and h is a parameter representing the amplitude of oscillations. For models 1 and II the maximum cavity size is $Z_0(1. + h)$ and $Z_0(1 + h)/(1 - h)$, respectively. In model I, the cavity is initially expanding at its highest velocity with the aerosol entrained so that the acceleration of the gas and the aerosol is always directed downwards from the upper boundary.

In model II, the gas and aerosol starts off at rest and a complete oscillation of the bubble is, considered in which the gas ends up again at rest in its initial configuration. Since the aerosol in the two models has the maximum and minimum gas velocities associated with oscillatory gas motion in a bubble, results from the two cases are expected to bracket possible behaviour in a realistic bubble under sodium where the initial aerosol motion is not uniquely specified.

For both models, calculations have been performed with $\omega = 50\ s^{-1}$ which is typical of the calculations performed by Jonas and Schütz (1988) (their Figure 7). They were made with the sodium data given in Appendix A and dimensionless equations given in Appendix B.

Results of impaction calculations for a complete oscillation in model I up to $\theta = \pi$ are shown in Figure 7 over the complete range of R for amplitude ratios h (see eq. (42)) from 1/4 to 4. The amount removed is negligible for R = 1 μm, but increases rapidly as R increases, reaching over 10% at R = 5 μm in 3 cases, and eventually reaching a type of plateau at large R.

The variation with geometry, which corresponds to maximum and minimum pressures reached in the bubble, is not quite as great as might be expected. As h changes by a factor of 16, the percentage of aerosol removed only increases by a factor of about 3.

In model I, the aerosol impacts the roof during the course of the oscillation, no empty regions appear, and the integrated percentage impacted is shown as a function of time in Figures 8 and 9. Initially, there is almost none as all the aerosol is assumed to be moving with the gas, but then the amount impacted steadily grows with time as shown in Figure 8 for different radii. At the maximum size of the cavity ($\theta = 90^0$), the percentages are already significant so that, although most of the aerosol impacts while the cavity is contracting ($\theta = 90\text{-}180^0$), the amount impacted during the expanding phase is not small.

The variation of the impaction percentage with h shown in Figure 9, shows no significant variation during the expansion-contraction cycle, the overall magnitudes not changing very much with h.
For calculations in model II, we chose the same range for R with values of h =`0.1,0.25,0.5` and `0.75` corresponding to oscillations which increase the size of the cavity by the factors, `11/9, 5/3, 3` and `7` respectively. The corresponding factors for model I with h = `0.25, 0.5,1, 2` and 4 are `5/4, 3/2, 2, 3` and `5,` respectively, so that the amplitudes in the two models correspond quite closely.

In Figure 10, we show total percentages of aerosol impacting as functions of radius and the maximum percentage of empty space that appears during the course of an oscillation. The major difference in model II from model I is that, because the top of the cavity accelerates upwards from rest, the aerosol is initially left behind and a space initially appears for all sizes. Impaction occurs during the second half of the cycle when the roof is moving down: this is noticeable in some of the PAROGA calculations reported by Jonas and Schütz (their Figure 6).

At the end of the cycle, an empty space usually reappears, and this is responsible for the strange behaviour of P_E with R shown for h = 0.75 in Figure 10. For small R, the maximum P_E appears at the end of the cycle, but for larger R the maximum occurs in the first half of the cycle, as is pointed out by the values of θ indicated at each side of the transition.

The changes of the impaction percentages with h are also rather surprising since, for small R, more aerosol is impacted with oscillations of small or moderate amplitude, as shown by the crossing of the curves in Figure 10. For large R, the total percentages impacted are a factor of 2 to 3 smaller than the analogous cases in model I shown in Figure 7.

The percentage occupancy of the cavity and the percentage of aerosol impacted during the oscillation are shown in Figure 11 for h = 0.5. Also indicated are the values of θ_m, the point where maximum impaction is reached, for the three values of R. After this point, an empty region reappears, but this barely happens for R = 30 μm, for which radius the percentage impacted is not much more than for R = 20 μm.

In Figure 12, we show a similar plot for different value of h with R = 15 gm, a radius for which the percentage impacted appears to peak at h near 0.5. For h = 0.75, less than 1% of the aerosol is impacted, and over half the cavity is again empty at $0 = 360^0$. This result suggests that there is an optimum amount of entrainment with which to eject particles by oscillating the surrounding gas. The values of θ_m found for the different values of h in Fig. 8 only span $\theta = 10^0$, whereas the span is 50^0 for the three values of R in Fig. 7.

The large variations in the percentage occupancy of the cavity shown in Figs. 11 and 12 are a general feature which shows that there would be considerable relative motion within the bubble between members of a polydisperse aerosol. This could lead to enhanced coagulation if the aerosol is dense.

Because of the large empty spaces within the bubble that appear in these model II calculations, the impaction results will not, in general, be independent of gravity. It is worth pointing out, however, that because there will be no similar spaces at the base of the cavity, the introduction of gravity can only increase the percentage impacted. This can easily be seen by considering the variation in the gap, Δz, shown in Fig. 6 when the top boundary does not meet the roof. Thus, the present calculations using model II give lower limits to impaction percentages.

6. Conclusions

Critical trajectories, which divide aerosol flows into distinct parts will appear in many areas of aerosol science where aerosol diffusion is relatively unimportant. Here we have described how they may be calculated in two very different cases. For impaction on fibres in filters, where gas flow fields must be calculated numerically, it will always be necessary to calculate trajectories numerically starting at an arbitrary possible point. We have shown that, by characterising the final boundary condition for a critical trajectory, there exists a very efficient iterative procedure, based on Newton's method, to calculate the starting point of the critical trajectory. We intend to use the method to investigate impaction on growing filter deposits, but its application is possible to many other cases involving impaction or the separation of gas streams. A particular example would be for air passing into the human respiratory system (Lai *et al* 2013). The passage can be divided into a number of sections such as the nasal passage and intervals between bifurcations in passages leading to the lungs, and various critical points involving large directional changes in the flow can be identified. Each of these points would have associated critical trajectories for particles passing them. To use the iterative procedure given in section 2 it would be necessary to identify a function associated with a limiting depositing trajectory which passes through zero at the point in question.

The second case concerns the application of the concept of critical trajectories to deposition in oscillating bubbles which was previously investigated in a possible practical case by Jonas and Schütz (1988). Here, we have shown that, where the gas velocity is a linear function of the space co-ordinate, but with an arbitrary time-dependence, the differential equation for a critical trajectory can be transformed into an integral equation. This enables their direct calculation without needing any iteration. The same mathematical transformation is applied to other types of bubble oscillation or oscillating cavities, and explicit results are given for radial volume oscillations of spherical bubbles.

The calculations reported here add the effects of gravity and changes to initial conditions to the work of Jonas and Schütz (1988) and support their conclusion that impaction would be an important mechanism for the removal of aerosol from a bubble formed in a HMA. For aerosol of over a few microns in size, the percentage removal rates found are quite large for a single oscillation. Since, for a dense aerosol, its mass would be concentrated at large sizes, the impaction mechanism alone would set limits to the amount of radioactive material which could be ultimately transmitted' through the sodium to the gas space.

We have seen that large regions of the bubble interior can become empty of aerosol of certain sizes during oscillations. This reflects on large relative velocities between small-sized aerosol (5 μm), which mainly follows the gas motion, and large particles. If the aerosol were dense enough, this motion would lead to a considerable amount of coagulation. It would be possible to use the present theory to calculate the relative velocities and coagulation rates.

The numerical results are consistent with those of Jonas and Schütz (1988) and generally show an expected behaviour in which the impaction percentage increases with both aerosol size and amplitude of oscillation of a bubble. This certainly applies to the first of our two models in which aerosol is initially entrained at the highest gas velocities during an oscillation. However, in the second model where the gas and aerosol start from rest, an interesting exception occurs. For aerosol below about 20 μm in size, a peak occurs in the impaction percentage as the amplitude of the oscillation increases. This unexpected result could be interpreted from Figure 12 as arising because the aerosol is partly entrained in the oscillation, but not enough to catch up with the motion of the top surface. Smaller size aerosol is more entrained initially, so that the proportion of empty cavity is smaller, and the aerosol impacts more when the top surface moves downwards in the second part of the oscillation. The peak in the coupling leading to impaction at a certain amplitude is reminiscent of resonant behaviour, and it would be very interesting to see it reflected in experiments.

It would be straightforward to extend the present theory to cases in which the bubble motion is specified numerically such as in simulations of HMA bubbles (Knowles and Turrel 1991). This would only involve using values of the initial velocity and the functions B(t) and f(t) provided numerically. The theory can also be applied to other types of bubble oscillation.

Acknowledgement

The original calculations for impaction in bubbles under sodium were funded by the Department of Trade and Industry.

References

Berthoud, G., Longest, A.W., Wright, A.L. and Schütz, W.P. (1988), Experiments on liquid-metal fast breeder reactor aerosol source terms after severe accidents. Nucl. Technol. 81, 257-277.

Davies, C.N. (1973) Aerosol Filtration, Academic Press, London.

Dunnett, S.J. and Clement, C.F. (2006) A numerical study of the efficiency of fibrous filters. *J. Aerosol Sci.* **37** 1116-1139.

Dunnett, S.J. and Clement, C.F. (2009) A numerical model of fibrous filter containing deposit. *Engineering analysis with Boundary elements* **33(5)** 601-610.

Dunnett, S.J. and Clement, C.F. (2012) Numerical investigation into the loading behaviour of filters operating in the diffusional and interception deposition regimes. *J. Aerosol Sci.* **53** 85-99.

Dunning, E.L. (1960), The thermodynamic and transport properties of sodium and sodium vapour ANL-6246.

Fink, J.K. and Leibowitz, L. (1979), Thermophysical properties of sodium. Argonne Report ANL-CEN-RSD-79-1.

Jonas, R. and Schütz, W. (1988), Motion and deposition of particles in expanding and oscillating gas bubbles. *J. Aerosol Sci.* 19, 753-765.

Knowles, J.B. and Turrel, M. (1991), The simulation of HMA vapour bubble dynamics. AEA-TRS-105

Lai, T.C., Marsi, Y.S. and Singh, M. (2008) Numerical of particle deposition in asymmetrical human airways under different inhalation cycles. *J. Mechanics in Medicine and Biology* **8** 55-74.

Lai, T.C., Marsi, Y.S., Das, S. and Owida, A. (2013) Numerical characterization of the flow field in a four-dimensional airway. *J. Mechanics in Medicine and Biology* **13** 1359968-(1-24).

Tu, J.Y., Yeoh, G.H., Morsi, Y.S. and Yang, W. (2004) A study of particle rebounding characteristics of a gas-particle flow over a curved wall surface. *Aerosol Sci. amd Tech.* **38** 739-755.

Vargaftik, N.B. (1975) Tables on the thermophysical properties of liquids and gases in normal and dissociated states. 2nd Ed. (Holstead Press)

Appendix A: Data for sodium

Most of the data quoted here is taken from Fink and Leibowitz (1979), but data from Dunning (1960) and Vargaftik (1975) have also been used. Fink and Leibowitz (1979) give the following expressions for the equilibrium vapour pressure, liquid density, latent heat of vaporisation, AHg, and equilibrium vapour density, ρ_{ve}, all as functions of absolute temperature T(K).

Equilibrium Vapour Pressure

$$p_{ve}(T) = 1.013\ 10^5 \exp[\ 18.832 - 13113/T - 1.09481nT + 1.977710^{-4}\ T]\ Pa \quad (A1)$$

$$dp_{ve}\ (T)/\ dT = p_{ve}(T)\ [13113/\ T^2 - 1.0948/\ T - 1.9777\ 10^{-4} \quad PaK^{-1} \quad (A2)$$

Liquid Density

$$\rho_\lambda\ = 1011.8 - 0.22054T - 1.9226\ 10^{-5}\ T^2 + 5.6371\ 10^{-9}\ T^3 \quad kg\ m^{-3} \quad T \le 1644\ K, \quad (A3)$$

$$= 214.1\ [\ 1 + 2.3709\ (1 - T/\ T_c)^{0.31645}\ + 2.8467\ 10^{-7}\ (\ T_c - T)^2 \quad kg\ m^{-3}\ 1644 \le T \le T_C, \quad (A4)$$

where T_c = 2509.46 K is the critical temperature.

Latent Heat

$$\Delta H_g\ (T) = 1.\ 4482\ 10^6\ (1 - T\ /\ T_c\ ) + 3.4849\ 10^6\ (1 - T\ /\ T_c)^{0.2} \quad J\ kg^{-1} \quad T\ \le 1644\ K \quad (A5)$$

$$= 1.8873\ 10^3\ T_C\ (1 - T/\ T_c\ )^{0.32227} \quad J\ kg\text{-}1 \quad 1644{:}5 \le T \le T_C \quad (A6)$$

Saturated Vapour Density

$$\rho_{ve}(T) = [\ \Delta H_g(T)\ /\ (\ T\ dp_{ve}\ (T)/\ dT) + 1\ /\ \rho_\lambda(T)\ ]^{-1} \quad kg\ m^{-3} \quad (A7)$$

Viscosity of Saturated Sodium Vapour

Sodium vapour or gas partly dimerizes so that no very simple expression can exist for the viscosity over a very large temperature and pressure range. Numerical values are given by Dunning (1960) for saturated sodium and these have been fitted by the simple expression,

$$\eta_v(T) = 5\ 10^{-8}\ T^{0.782} \quad Ns\ M^{-2}, \quad (A8)$$

over the temperature range from 500^0C (773K) to 1300^0C (1573K) to an accuracy of better than 4%.

The values given are about a factor of 2 smaller than those quoted by Vargaftik (1975) for monatomic sodium vapour, which nevertheless show that the viscosity has only a weak dependence on pressure for superheated vapour.

If required, the kinematic viscosity at saturation is given by

$$\nu_v(T)\ =\ \eta_v(T)\ /\ \rho_{ve}(T) \quad m^2\ s^{-1}.$$

Appendix B. Dimensionless Equations

In terms of the dimensionless variables, $\theta\ =\ \omega t$, $p = \alpha\ /\ \omega$, we rewrite eq. (21) as

$$dX\ /\ d\theta = p\ I\ (\theta) \quad (B1)$$

$$I\ (\theta) = \int_0^\theta d\theta'\ \exp\ [-p(\theta - \theta')]\ [B(\theta') + X(\theta')l\ f\ (\theta') \quad (B2)$$

For the two models I and II, the functions B (θ) and f (θ) with corresponding subscripts 1 and 2, respectively, are given explicitly by:

$$B_1(\theta) = 1 + (\ h\ /\ p)(\ 1 - \exp(-p\ \theta)) \quad (B3)$$

$$f_1\ (\theta) = h\ \cos\ \theta\ /\ (\ l + h\ \sin\ \theta), \quad (B4)$$

$$B_2\ (\theta) = l, \quad (B5)$$

$$f_2(0) = h\ \sin\ \theta\ /\ (\ 1 - h\ \cos\ \theta'). \quad (B6)$$

Clearly p, with α given by eqs. (11) and (12), is the most important parameter in determining whether aerosol follows the bubble oscillations. For our calculations with R from 1 to 30 μm, p varies from 268 to 0.298, and satisfactory numerical integration of eqs. (B1) and (B2) was found not to be straightforward, particularly for large p, because of the exponent in (B2). Accordingly, a hybrid numerical scheme was adopted, which was found to be satisfactory in stepping forward the function x (θ) in θ or time:

$$\theta_{n+1} = \theta_n + \delta\theta, \tag{B7}$$

$$X(\theta_{n+1}) = X(\theta_n) - (\exp(-p\delta\theta) - 1)\,[I(\theta_n) + \tfrac{1}{2}\,\delta\theta\, F(\theta_n)], \tag{B8}$$

$$F(\theta_n) = f(\theta_n)\,[B(\theta_n) + X(\theta_n)], \tag{B9}$$

$$I(\theta_{n+1}) = \exp(-p\delta\theta)\, I(\theta_n) + \tfrac{1}{2}\delta\theta\,[F(\theta_{n+1}) + \exp(-p\delta\theta)F(\theta_n)] \tag{B10}$$

In model I, θ runs from 0 to π and in model II from 0 to 2π..

Figure Captions

Fig. 1. Critical trajectory for impaction on a filter fibre.

Fig. 2. Negative distance used for R_{min} for an impacting trajectory.

Fig. 3. Values of y_0 obtained for successive iterations: y_0 = y1 for case A with St = 1.0899 and y_0 = y2 for case B with St = 5.

Fig. 4. Corresponding values of $y = y_0$ and R_{min} for successive iterations in case A starting at $y_0 = 1$.

Fig. 5. Cavity Height, Z(t), and critical trajectory, z(t), as functions of time. (a) The trajectories in the shaded area, starting between $z = z_0$ and Z_0, will all have impacted into the wall at time t. (b) Limiting trajectopries when empty regions appear. Impaction takes place between T_i and t_m.

Fig. 6. Identical fractions (shaded) of initial aerosol removed by impaction with and without gravity in one-dimensional vertical motion.

Fig. 7. Percentage, P_i, of initial aerosol of radius R impacting the roof for an oscillation in model I with mplitude ration h and time 0.063 s.

Fig. 8 Percentage, P_i, of initial aerosol impacting the roof in model I as a function of time, $\theta = \omega t$, for different aerosol radii, R(μm).

Fig. 9. Percentage, P_i, of initial aerosol impacting the roof in model I as a function of time, $\theta = \omega t$, during the oscillation of amplitude h.

Fig. 10. Percentage, P_i, of initial aerosol impacting the roof for an oscillation in model II with amplitude h, and maximum percentages, P_E, of cavity empty during the oscillation.

Fig. 11. Percentage, P_i, of initial aerosol impacting the roof, and percentage, P_O, of the cavity occupied in model II as functions of time, $\theta = \omega t$, for different radii and h = 0.5.

Fig. 12. As for Fig. 11 for different h with R = 15 μm.

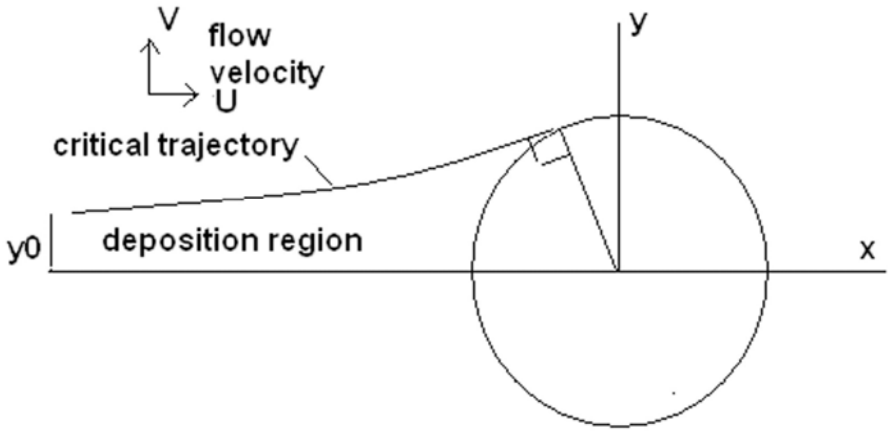

Fig 1

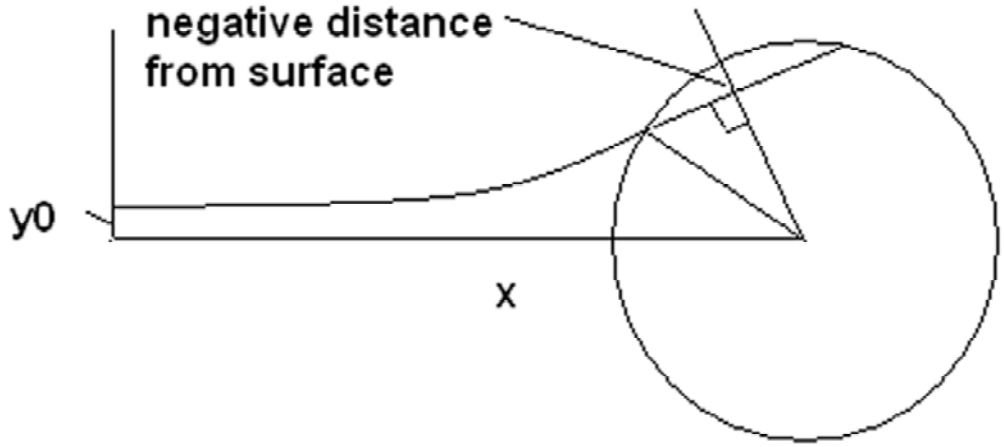
negative distance
from surface
y0
x

Fig 2

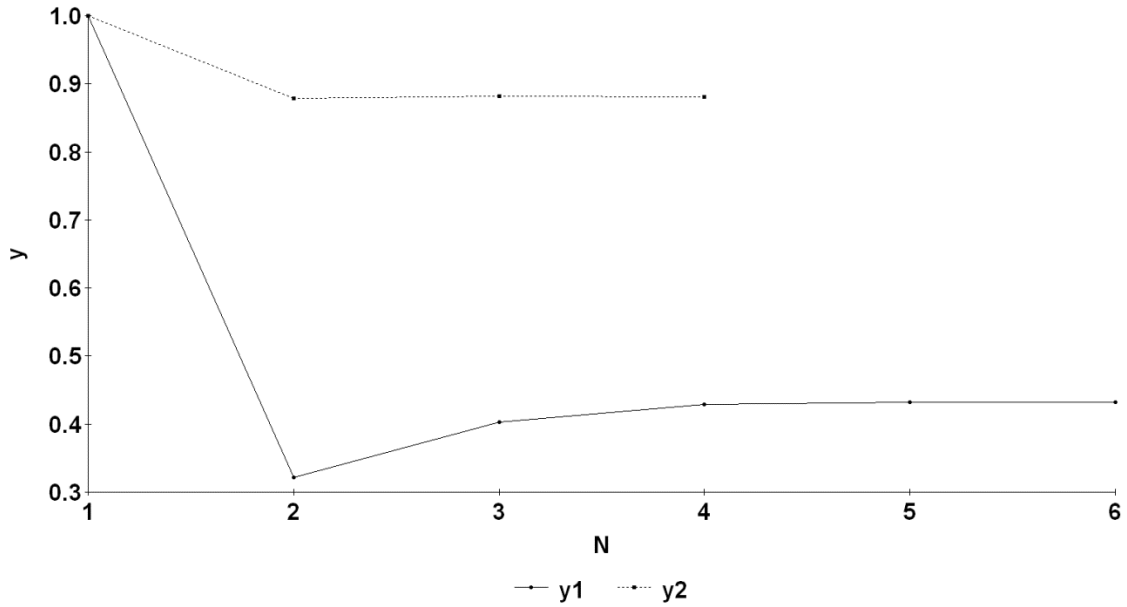
1.0
0.9
0.8
0.7
0.6
0.5
0.4
0.3
y
1
2
3
4
5
6
N
y1
y2

Fig 3

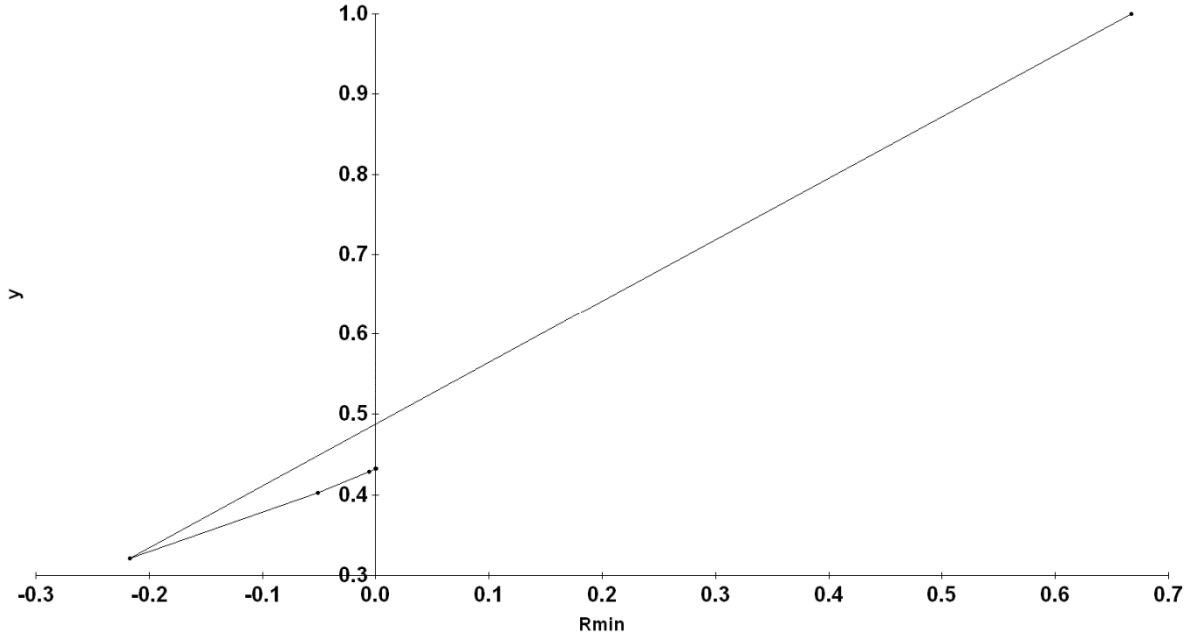

Fig 4

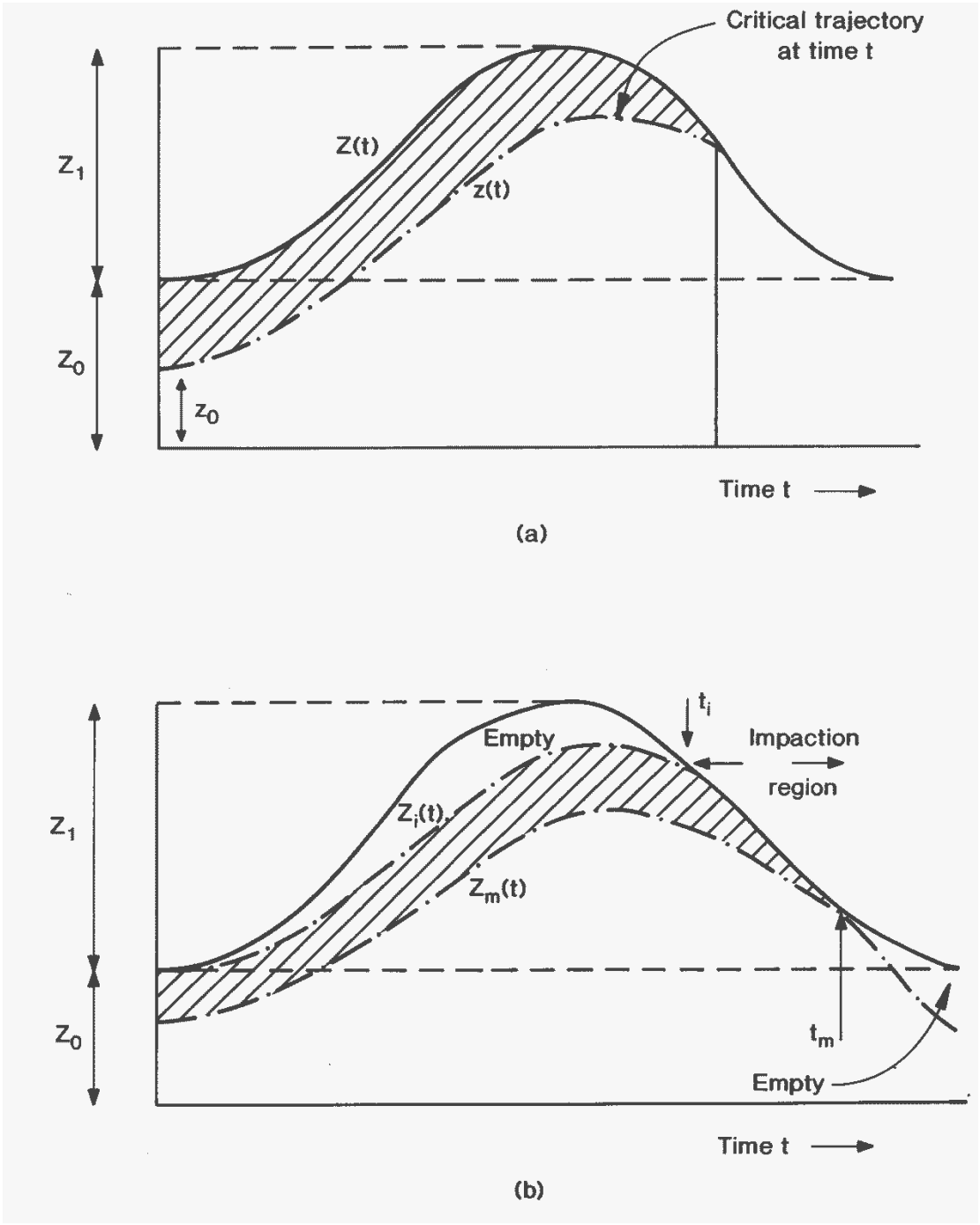
Critical trajectory
at time t
Z(t)
z(t)
Z_1
Z_0
z_0
Time t
(a)
t_i
Empty
Impaction
region
$Z_i(t)$
$Z_m(t)$
Z_1
Z_0
t_m
Empty
Time t
(b)

Fig 5

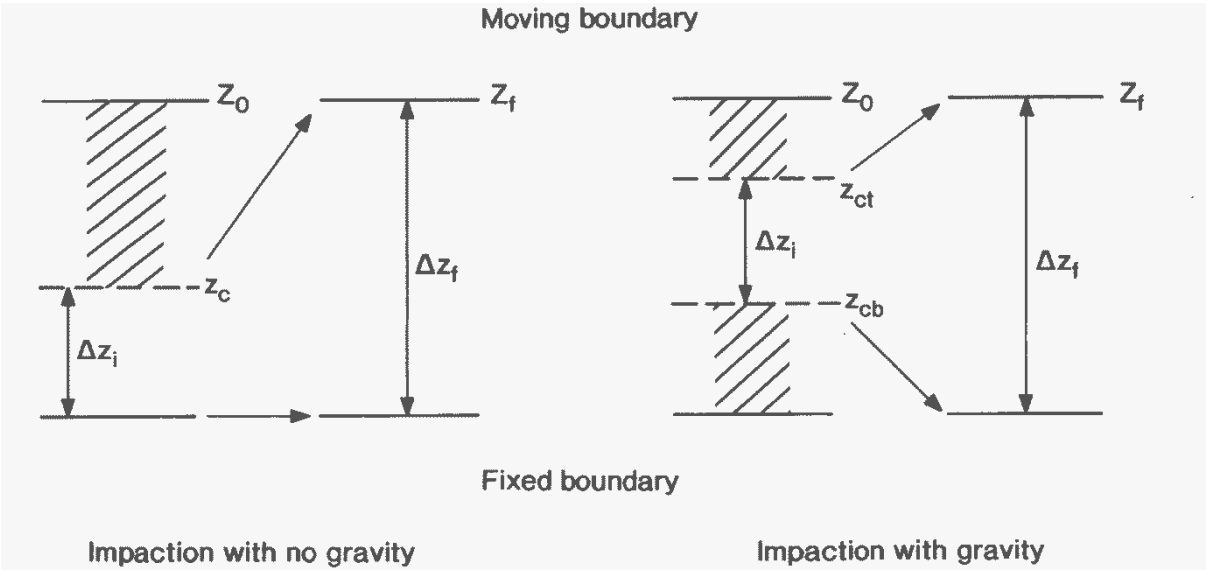
Moving boundary
Z_0
Z_f
z_c
Δz_f
Δz_i
Z_0
Z_f
z_{ct}
Δz_i
Δz_f
z_{cb}
Fixed boundary
Impaction with no gravity
Impaction with gravity

Fig 6

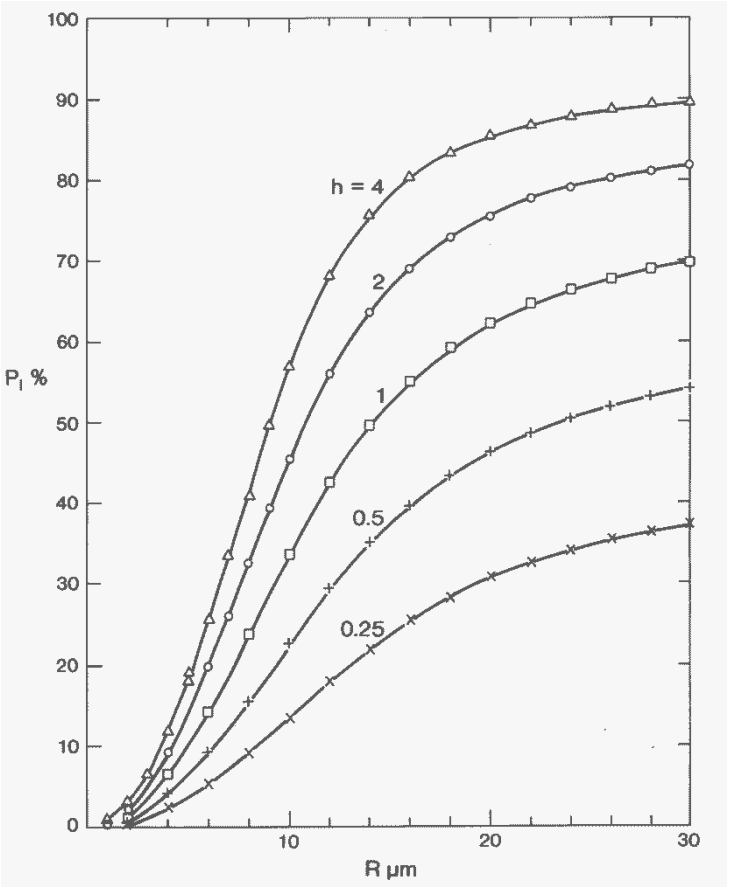
100
90
80
70
60
50
40
30
20
10
0
P_i %
h = 4
2
1
0.5
0.25
10
20
30
R μm

Fig 7

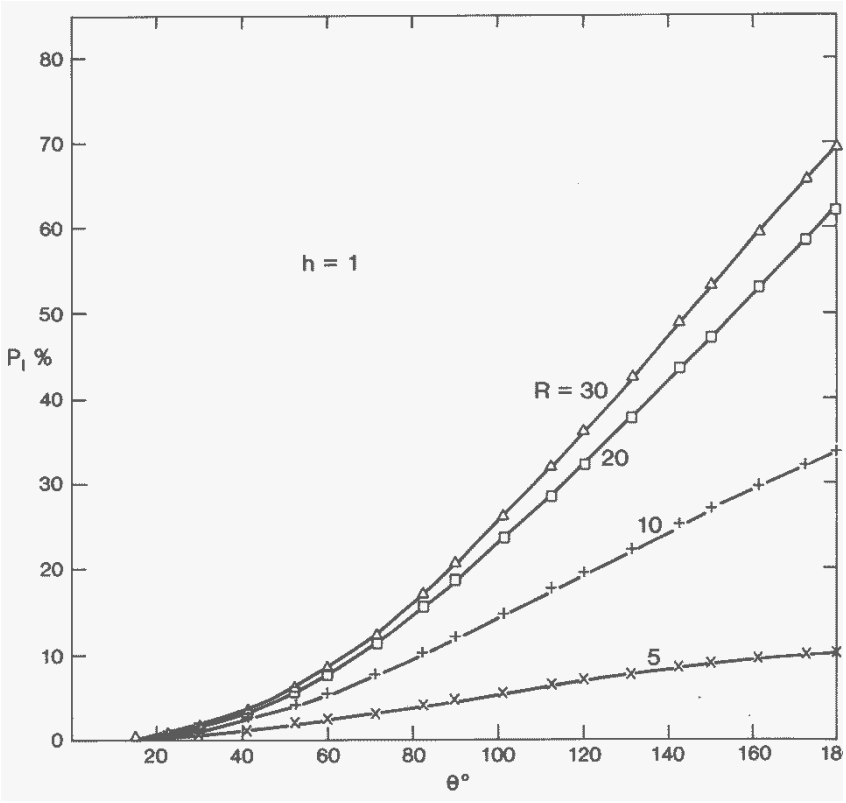

Fig 8

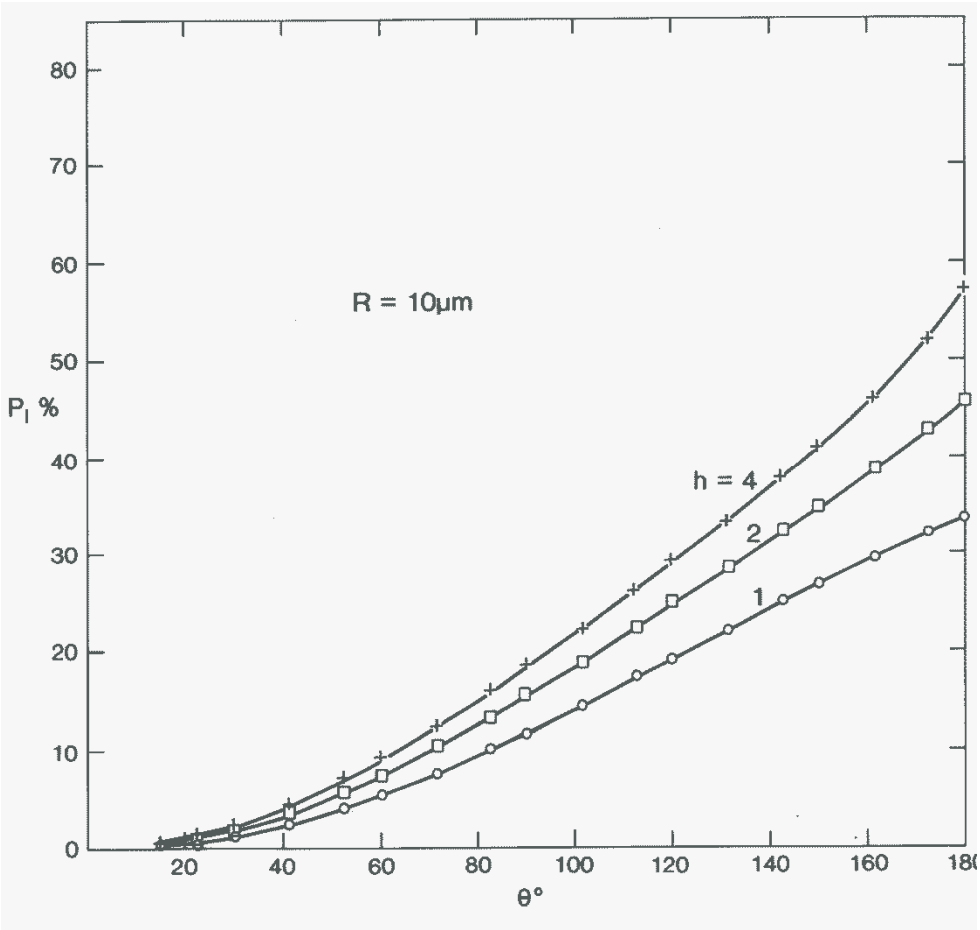

Fig 9

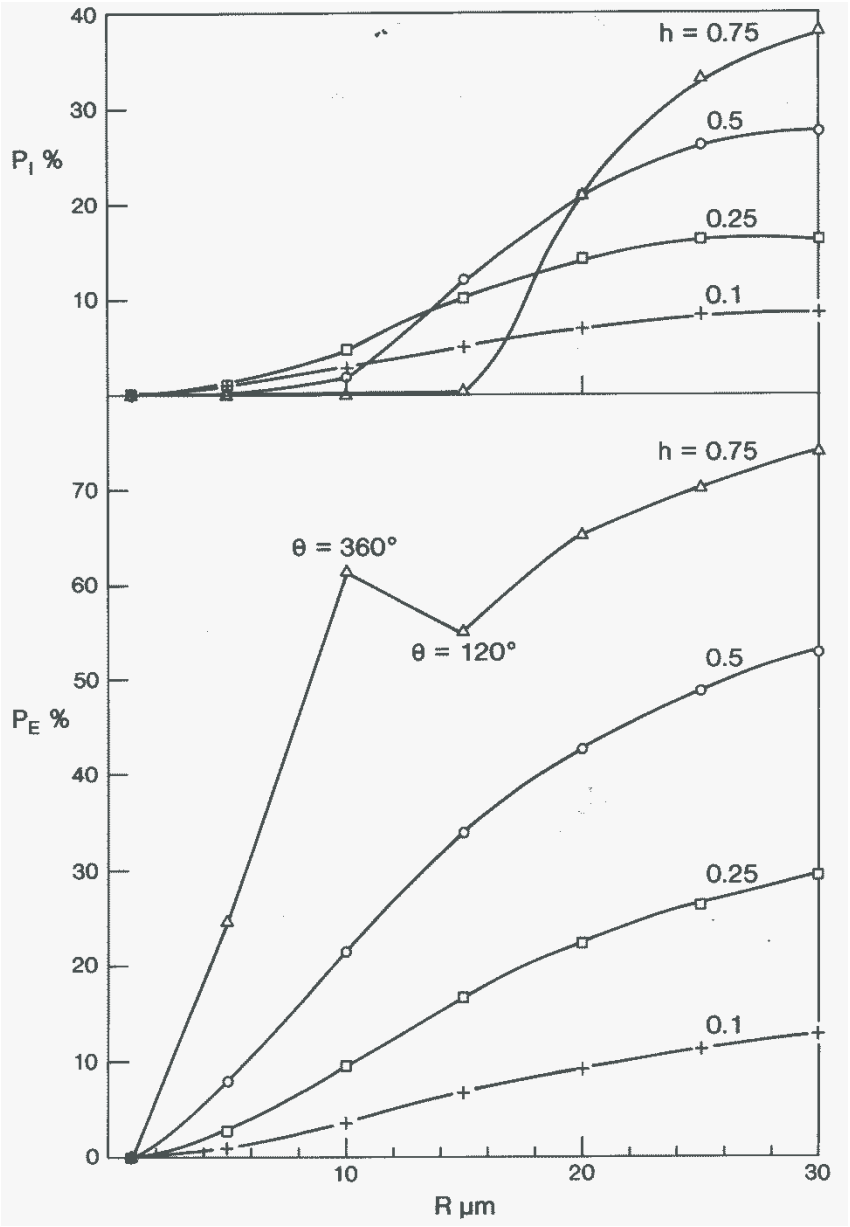
h = 0.75
0.5
0.25
0.1
P_I %
40
30
20
10
h = 0.75
θ = 360°
θ = 120°
0.5
0.25
0.1
P_E %
70
60
50
40
30
20
10
0
10
20
30
R µm

Fig 10

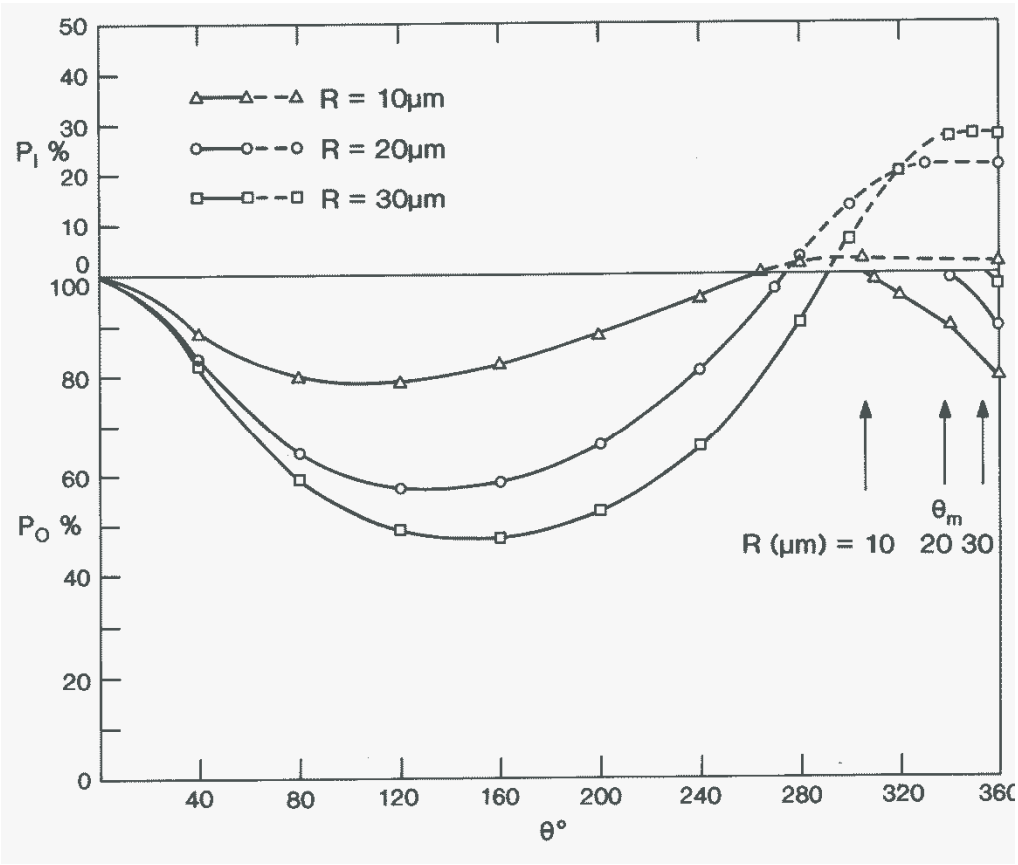
R = 10μm
R = 20μm
R = 30μm
P_I %
P_O %
θ°
$θ_m$
R (μm) = 10 20 30

Fig 11

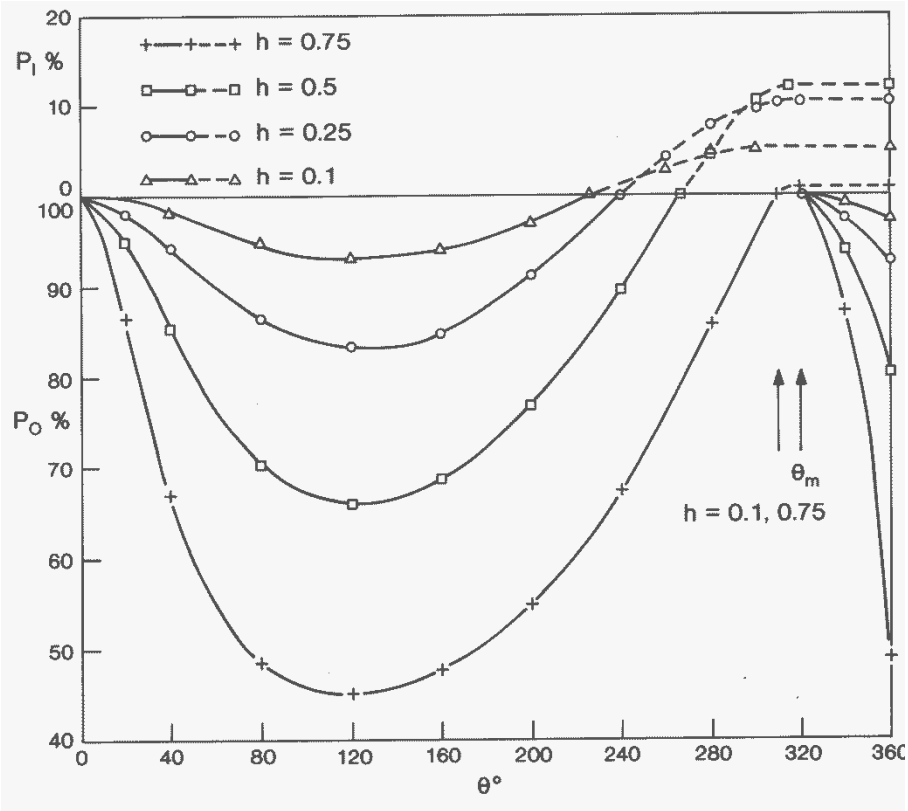
h = 0.75
h = 0.5
h = 0.25
h = 0.1
P_I %
P_O %
θ°
$θ_m$
h = 0.1, 0.75

Fig 12